Large-scale structure in a new deep IRAS galaxy redshift survey

Article (Published Version)

Mon. Not. R. Astron. Soc. **000**, 000–000 (0000) Printed 23 January 2014 (MN LATEX style file v1.4)

Large Scale Structure in a new deep IRAS galaxy redshift survey

S.J. Oliver[1], M. Rowan-Robinson[1], T.J. Broadhurst[2], R.G. McMahon[3], W. Saunders[4], A. Taylor[5] A. Lawrence[5], C.J. Lonsdale[6], P. Hacking[6], and T. Conrow[6]

[1] *Imperial College of Science Technology and Medicine, Blackett Laboratory, Prince Consort Road. London SW7 2BZ.*
[2] *Johns Hopkins University, Johns Hopkins Road, Laurel, MD 20723-6099, USA.*
[3] *Institute of Astronomy, Madingly Road, Cambridge CB3 0HA.*
[4] *Department of Astrophysics, Keeble Road, Oxford OX1 3RH.*
[5] *Institute for Astronomy, Blackford Hill, Edinburgh EH9 3HJ.*
[6] *IPAC, California Institute of Technology, 770 South Wilson Avenue, Mail Code 100-22, Pasadena, CA 91125, USA.*

Accepted 1995 November 16. Received 1995 November 1; in original form July 12

ABSTRACT

We present here the first results from two recently completed, fully sampled redshift surveys comprising 3703 IRAS Faint Source Survey (FSS) galaxies. An unbiased counts-in-cells analysis finds a clustering strength in broad agreement with other recent redshift surveys and at odds with the standard cold dark matter model. We combine our data with those from the QDOT and 1.2 Jy surveys, producing a single estimate of the IRAS galaxy clustering strength. We compare the data with the power spectrum derived from a mixed dark matter universe. Direct comparison of the clustering strength seen in the IRAS samples with that seen in the APM-Stromlo survey suggests $b_O/b_I = 1.20 \pm 0.05$ assuming a linear, scale independent biasing. We also perform a cell by cell comparison of our FSS-z sample with galaxies from the first CfA slice, testing the viability of a linear-biasing scheme linking the two. We are able to rule out models in which the FSS-z galaxies identically trace the CfA galaxies on scales 5-20h^{-1}Mpc. On scales of 5 and 10h^{-1}Mpc no linear-biasing model can be found relating the two samples. We argue that this result is expected since the CfA sample includes more elliptical galaxies which have different clustering properties from spirals. On scales of 20h^{-1}Mpc no linear-biasing model with $b_O/b_I < 1.70$ is acceptable. When comparing the FSS-z galaxies to the CfA *spirals*, however, the two populations trace the same structures within our uncertainties.

Key words:
galaxies: clusters: general – galaxies: elliptical & lenticular, cD – galaxies: spiral – large-scale structure of Universe – infrared: galaxies

1 INTRODUCTION

Following the success of IRAS Point Source Catalog (PSC) galaxy redshift surveys in probing the large scale structure of the local Universe, which presented serious problems for the standard cold dark matter (CDM) theory (Efstathiou *et al.*1990; Saunders *et al.*1991; Kaiser *et al.*1991; Moore *et al.*1992; Strauss *et al.*1992; Fisher *et al.*1993) two new fainter redshift surveys have been undertaken to confirm these results at significantly greater depths.

The first of these surveys (FSS-z I[⋆]) was based on samples drawn from the IRAS Faint Source Data Base [FSDB, see Moshir *et al.* (1992)]. On the basis of deep IRAS coverage and freedom from cirrus contamination, three regions in the Northern Galactic Hemisphere were selected (these areas are defined in Table 1). Within these areas we believe the FSDB to be $\sim$ 99 per cent complete for $S_{60} \geq 0.2$ Jy (Lonsdale *et al.* in preparation). We thus constructed a cat-

⋆ These surveys have been referred to previously as 'QCCOD'

Table 1. Definition of FSS-z areas. Areas N, A and E constitute FSS-z I while P and X constitute FSS-z II.

	Definition		Area/ sq deg
N	$150\,\mathrm{deg} \le l \le 210\,\mathrm{deg}$,	$50\,\mathrm{deg} \le b \le 70\,\mathrm{deg}$	594
A	$30\,\mathrm{deg} \le l \le 90\,\mathrm{deg}$,	$60\,\mathrm{deg} \le b \le 68\,\mathrm{deg}$	178
E	$70\,\mathrm{deg} \le l \le 90\,\mathrm{deg}$,	$50\,\mathrm{deg} \le b \le 55.5\,\mathrm{deg}$	67
P	$26.5\,\mathrm{deg} \le \delta \le 44.5\,\mathrm{deg}$,	$b \ge 70\,\mathrm{deg}$ if $\alpha \le 12^h$ or $b \ge 68\,\mathrm{deg}$ if $\alpha > 12^h$	476
X	$32.5\,\mathrm{deg} \le \delta \le 38.5\,\mathrm{deg}$,	$b < 50\,\mathrm{deg}$ & $\alpha \ge 8^h$	94

alogue of all FSDB sources within these areas having good to moderate 60μm fluxes greater than 0.2 Jy. (In area E an additional sample was selected with $0.15 \le S_{60} < 0.2$ but this is not considered further in this paper.) The majority of such sources are galaxies [e.g. Rowan-Robinson *et al.* (1986), Lawrence *et al.* (1986)]. No formal colour-cuts were employed to exclude either stars or cirrus sources. The former were excluded upon inspection of the POSS plates or APM cartoons together with a case by case examination of the colours. In the combined FSS samples only five 'stars' lay close to the galaxy colour locus and they had the same colours as the 60μm excess stars. In addition 13 galaxies were excluded because a bright star lay in the field making identification and acquisition impossible, these are assumed to be random line of sight coincidences with little effect on our analysis. Cirrus sources were rare because of our careful selection of areas (four sources have been excluded upon examination of maps made from the raw IRAS data). This survey was particularly designed to clarify the evolutionary behaviour of the IRAS population; see contrasting conclusions of Saunders *et al.*(1990) and Fisher *et al.* (1992).

The second survey (FSS-z II) was constructed from the Faint Source Catalog Version 2 (Moshir *et al.*1992). The area selected traversed the North Galactic Pole connecting the FSS-z I areas. In other respects the FSS-z II samples were selected in the same manner as FSS-z I. Designed principally for large scale structure studies, the flux completeness in areas P and (to a lesser extent) X is not as good as other areas and is estimated to be 90 per cent at 0.25 Jy.

The combined surveys cover an area of 1310 deg^2 (0.4 sr) and contain 3728 sources, more than 3600 of which are galaxies.

Redshifts were obtained from the literature for 872 sources; a number of redshifts were kindly provided in advance of publication by: John Huchra, Ray Wolstencroft, Quentin Parker & Roger Clowes and Marc Davis & Michael Strauss. Major observation programmes were instigated to obtain the redshifts for the remaining sources using the FOS and FOS2 instruments on the INT and WHT facilities. Using automatic, optimal extraction techniques and line fitting procedures we obtained an average redshift accuracy of $\sim 190\mathrm{km\,s^{-1}}$ (Oliver 1993, and Oliver *et al.*in preparation), c.f. an accuracy of $\sim 250\mathrm{km\,s^{-1}}$ for the QDOT survey (Lawrence *et al.*, in preparation).

Of all 1931 FSS-z I galaxies we currently have 1769 redshifts giving an overall redshift completeness of 91.6 per cent; while for the FSS-z II project we have redshifts for 80.4 per cent of the galaxies. A mask has been constructed which, as well as defining the survey boundaries, excludes a number of sectors that have not been exhaustively followed up and those sources lying close to the IRAS coverage gap. Upon application of this mask the completeness statistics improve to 92.5 per cent and 86.8 per cent respectively. Above 0.25Jy (where FSS-z II suffers less from flux incompleteness) we have 95 per cent of the FSS-z I redshifts and 90 per cent for FSS-z II. Detailed numbers are listed in Table 2. Of the failures the most interesting will be those with either very faint or no optical counterparts. VLA maps have been obtained for all sources in the FSS-z I that are either blank within the IRAS error ellipse (to the limit of the sky survey plates) or have very faint identifications. R-band CCD images have also been obtained for many of these sources. These have yielded a number of further identifications and redshifts have been obtained for several of these. Work is continuing to obtain the redshifts for the remainder.

Table 2. Redshift completeness statistics. The subsample has sources lying within our 'mask' excluded. Figures in parenthesis indicate the number of galaxies for which we have redshifts.

	Total	galaxies		subsample		$S_{60} > 0.25$Jy	
N	1410	1369	(1253)	1369	(1253)	924	(874)
A	474	457	(413)	383	(361)	263	(251)
E	107	105	(103)	105	(103)	71	(70)
P	1416	1391	(1133)	1234	(1062)	921	(826)
X	321	312	(236)	224	(203)	146	(134)
	3728	3634	(3138)	3315	(2982)	2325	(2155)

This paper quantifies the large scale clustering seen in both surveys and directly compares these samples with optical surveys. These surveys are also being used for many other studies. It was during the first of these projects that the unique object F10214+4724 was discovered (Rowan-Robinson *et al.*1991). The completeness and reliability of the FSS-z I survey will be detailed in future papers (Lonsdale *et al.*& McMahon *et al.*, in preparation). Simple tests reveal significant evolution within this sample (Oliver *et al.*1995). This evolution will be elaborated in greater detail by Broadhurst *et al.*(in preparation). The appearance of the Boötes void which overlaps with areas A & E will be discussed by Oliver *et al.*(in preparation). The data for both surveys will be presented by Oliver *et al.* (in preparation).

2 COUNTS-IN-CELLS

To assess the large scale structure seen in the FSS-z surveys quantitatively we have chosen to apply the counts-in-cells method described by Efstathiou *et al.*(1990, ; hereafter E90) and also used by Loveday *et al.* (1992). The two-point autocorrelation function is a useful descriptive statistic; indeed for Gaussian fields it provides a complete statistical profile of the field. The counts-in-cells method measures a volume integral of this function, the variance, and avoids the problem of assigning weight to galaxies in direct measurements of the two-point correlation function This analysis is also relatively straightforward to perform in the presence of a mask covering a significant fraction of the sky, a considerable advantage over direct determinations of the power-spectrum in Fourier space.

2.1 Basic Method

We consider the moments of galaxy counts (N_i) over a lattice of M cells. Following E90 we define the statistics

$$\bar{N} = \frac{1}{M}\sum_i N_i \quad (1)$$

$$S = \left(\frac{1}{(M-1)}\sum_i (N_i-\bar{N})^2\right) - \bar{N}. \quad (2)$$

The statistic $\bar{N}$ has an expectation value nV, where n is the mean galaxy density and V is the cell volume. *If* the cells are independent then the expectation value of S, $\langle S\rangle = n^2\sigma^2V^2$, where σ^2 is a volume integral over the two-point autocorrelation function:

$$\sigma^2(l) = \frac{1}{V^2}\int_{V_1V_2=l^3}\xi(r_{12})dV_1dV_2. \quad (3)$$

σ^2 is also closely related to the power spectrum as described in Section 2.4.

If the cells are independent and the number of cells is large then we can derive an expression for the variance of S [var(S)] in terms of the first four moments of the density field (equation 4 in E90). However, if we assume Gaussian fluctuations then the higher order reduced correlation functions vanish giving

$$\mathrm{var}(S) = \frac{2n^2V^2(1+\sigma^2)+4n^3V^3\sigma^2+2n^4V^4\sigma^4}{M}. \quad (4)$$

This allows us to estimate var(S) for a given sample by using the empirical estimates $nV \approx \bar{N}$ and $\sigma^2 \approx S/\bar{N}^2$ in equation 4. For non Gaussian fluctuations this underestimates the errors and ideally we should use N-body simulations of a particular model to determine higher order moments and thus estimate the errors.

A survey volume is divided up into concentric shells and these are then divided into M_i cells. The mean number density of the cells is constant within a given shell allowing density estimations of the variance from each shell. These estimates can be combined using the maximum likelihood technique. The statistics N_i and S_i are calculated for each shell and we construct the likelihood function from all shells

$$\mathcal{L}(\sigma^2) = \prod_i \frac{1}{[2\pi\mathrm{var}(S_i)]^{1/2}}\exp\left[-\frac{(S_i-n_i^2V^2\sigma^2)^2}{2\mathrm{var}(S_i)}\right]. \quad (5)$$

We can now estimate σ^2 by replacing $n_i^2V^2$ with $\bar{N}_i^2$ and maximizing the likelihood function numerically. We can justify not using a joint likelihood function for the two estimators, $\bar{N}_i^2$ and S_i, since the errors in $\bar{N}_i^2$ are much smaller. The 68 per cent confidence limits to this maximum likelihood solution are the values of σ^2 where the log likelihood has dropped by a factor of 0.5 from its maximum value. This maximum likelihood technique automatically weights the shells, shells with few cells or sparse density receiving less weight.

To determine how well the data are modelled by our maximum likelihood solution we also calculate the χ^2 of each fit,

$$\chi^2 = \sum\frac{(S_i-\bar{N}_i^2\sigma^2)^2}{\mathrm{var}(S_i)} \quad (6)$$

where the number of degrees of freedom (ν) is one less than the number of shells.

2.2 Detailed Method

In this Section we discuss finer points of the counts in cells method. Specifically we propose two refinements to the method of E90.

In practice each cell does not have exactly the same volume owing to the non-uniform mask. We correct the estimators $\bar{N}$ and S for incomplete volumes as prescribed by equation 9 in E90 (N.B. equation 9 in E90 has a minor typographical error) i.e.

$$\bar{N} = \frac{\sum N}{\sum V} \quad (7)$$

$$S = \frac{\sum\left(N-\bar{N}V\right)^2 - \left[1-\frac{\sum V^2}{\left(\sum V\right)^2}\right]\sum N}{\bar{N}^2\left[\sum V^2 - 2\frac{\sum V^3}{\sum V}+\frac{\left(\sum V^2\right)^2}{\left(\sum V\right)^2}\right]}. \quad (8)$$

This correction only takes into account the fact that the expected number of galaxies in a restricted cell will be reduced. In addition, a masked cell will, in general, sample smaller scales. Since it is observed that clustering is stronger on smaller scales this means that the expected σ^2 increases. This bias is difficult to correct for since it depends in detail on the topology of the mask and the slope of the correlation function. We have elected simply to exclude those cells with more than half the volume masked.

At large distances the number of galaxies per cell has dropped significantly so that we no longer get a meaningful addition to our estimate of the variance. E90 showed that if $\bar{N}\sigma^2 \gg 1$ the variance is inversely proportional to the volume. Similarly it can be shown that if $\bar{N}\sigma^2 \ll 1$ and $\bar{N} \ll 1$ the variance on σ^2 actually increases with additional cells. Thus $\bar{N}\sigma^2 = 1$ represents some measure of useful depth of a survey (not surprisingly this is where the Poisson variance equals the clustering variance). Although the maximum likelihood analysis includes a weighting scheme there is little point in taking shells much beyond this limit. We estimate this depth using σ^2 from E90 and the luminosity function of Saunders *et al.* (1990) and only consider shells to roughly twice this depth.

It has been claimed that the counts-in-cells method as it stands is independent of the galaxy selection function [E90, Efstathiou (1995)]. This is not strictly true. Since the selection function is not constant across each shell the galaxies will tend to be concentrated towards the nearest side. This reduces the effective volume of the cells and (as with masking) will bias the variance upwards. With prior knowledge of the clustering strength and selection function one could estimate and remove this bias. Instead of this we eliminate this bias by volume limiting each shell (i.e. removing all galaxies that would not have been visible if placed at the far side of their shell). The removal of galaxies should not seriously affect our final errors since they are not sensitive to the mean

density. As expected this correction reduces the variance in almost every case. For QDOT in particular the reduction was considerable, up to 1.7 times the quoted errors. Comfortingly the χ^2 usually decreased, showing that the fit was better.

We found that the variances obtained by the counts-in-cells method were quite sensitive to the specific grid pattern used. To reduce this sensitivity we use 16 different grids for each survey. First we divide the volumes into equal thickness concentric shells, then divide these shells with latitude and longitude cuts such that the resulting cells have equal volumes (in the absence of any mask). These latitude and longitude cuts are then offset by 1/2 and 1/4 spacing in both dimensions to produce eight different grids. This entire process is then repeated with the shells offset by 1/2 a shell thickness. Each grid gives us 1σ upper and lower limits to the variance. We take the linear average of these over the 16 grids to produce a final estimate of the upper and lower limits on the variance. In the process we also produce an estimate of the scatter between the individual grids; in many cases it is comparable to our quoted errors. By averaging over 16 different grids we have thus undoubtedly reduced the errors. It would be possible to account for the reduction in systematic errors by subtracting the grid error (estimated from the scatter between different grids) in quadrature from the maximum likelihood error estimate. However, in some cases our grid error is actually larger than our maximum likelihood error, and this procedure would lead to negative variances. This is a further indication that the maximum likelihood errors are underestimated. So a correction for the reduction in systematic errors due to the re-gridding is not possible without using full non-Gaussian error estimates. Figure 1 shows σ^2 for each of the 16 grids used for our FSS-z surveys together with the final averaged results.

To assess the goodness of the maximum likelihood solutions we also sum up the χ^2 and ν over all grids. Since variances determined from the shells of one grid are *not* independent from the shells in another grid we have overestimated the number of degrees of freedom, hence the overall goodness of fit will be optimistic.

In equation 5 we estimate $n_i^2 V^2$ with the biased estimator $\bar{N}_i^2$. We have investigated replacing $\bar{N}_i^2$ with the unbiased estimator $[(\sum_i N)^2 - \sum_i N^2]/M(M-1)$ but did not find any significant differences.

A further bias arises because the cells are not independent. As discussed by E90 and Loveday *et al.* (1992) this affects the estimate of var(S). However, correlations between cells also bias the estimator S downwards. Ideally each shell should include many uncorrelated volumes. A small area survey will have fewer uncorrelated cells per shell than a large area survey of the same volume. We thus might expect our FSS-z to show less variance than the all sky surveys and since we do not see such an effect we assume that this bias is small.

2.3 Results

We apply the above method to our new surveys and also to existing IRAS redshift surveys: the latest version of the QDOT survey (Lawrence *et al.* in preparation); the 1.2 Jy survey (Fisher *et al.*1995); a faint QDOT sample (0.6-1.2 Jy); a combined PSC (QDOT and 1.2 Jy) sample. We also combine our FSS-z sample with the combined PSC sample to produce a single IRAS sample.

Figure 1. σ_i^2 as a function of cell dimensions (l) for each of the 16 grids of the FSS-z surveys (error bars not plotted). Also shown is the average of these 16 with averaged error bars

For our FSS-z surveys we flux limit the whole sample at 0.25Jy to allow for the varying completeness limits in different areas. The mask was described in Section 1.

For the QDOT and faint QDOT samples we use the standard QDOT mask. The faint QDOT sample has $0.6 < S_{60} < 1.2$ Jy so the volume limiting is rather harsh.

In the analysis of the 1.2 Jy sample we apply a cut of $|b| > 5\,\mathrm{deg}$ together with the QDOT mask. This is slightly more severe than the 1.2 Jy team used themselves.

Since the faint QDOT sample has no galaxies in common with the 1.2 Jy survey the two can be combined to construct a larger PSC sample. For this PSC sample we use the same mask as we used for the 1.2 Jy catalogue. Many fewer galaxies are excluded when volume limiting the combined PSC sample than are excluded when volume limiting the samples separately.

Finally, we take the individual variance estimates from each shell of our combined PSC sample, together with the individual variances from each shell of our FSS-z sample, to construct a single likelihood function (equation 5), as before. Maximizing this likelihood function gives us a single variance estimate from all samples. Since the volume of overlap between the FSS-z and the PSC is small, any interdependence will not be a significant problem.

The results for all the various samples described above are given in Table 3.

In many cases the χ^2 and ν values indicate that the goodness of fit for the individual grids is poor. As discussed in E90 the assumption of Gaussian fluctuations causes the errors to be underestimated which may explain this. Since we reduce the systematic errors by averaging over 16 grids, without adjusting our error estimates accordingly we have to some extent compensated for this.

The QDOT variances appear slightly smaller than those quoted by E90 and Efstathiou (1995). The main reason for this is that by volume limiting each shell we have removed the bias due to gradients in the selection function. The grids also play a part in this apparent discrepancy; without vol-

Table 3. σ^2 for the various samples, averaged over 16 grids in each case. Including χ^2 and grid scatter estimate

l	σ^2	χ^2	ν	$P(\chi^2,\nu)$	$\sigma_{\rm GRID}$
		FSS-z Samples			
10	0.863 ± 0.097	296	251	2.762	0.056
20	0.322 ± 0.059	338	251	0.020	0.050
30	0.172 ± 0.053	402	235	0.000	0.070
40	0.182 ± 0.070	320	203	0.000	0.063
60	0.095 ± 0.053	105	107	53.387	0.087
		QDOT Sample			
10	0.716 ± 0.108	133	104	3.026	0.073
20	0.308 ± 0.061	123	88	0.831	0.074
30	0.199 ± 0.054	137	72	0.001	0.038
40	0.127 ± 0.041	111	72	0.239	0.048
60	0.069 ± 0.030	34	40	73.224	0.045
		QDOT Faint($S_{60} < 1.2$ Jy) Sample			
10	0.811 ± 0.365	111	72	0.209	0.432
20	0.709 ± 0.288	72	56	7.358	0.286
30	0.392 ± 0.311	46	40	24.406	0.391
40	0.152 ± 0.337	28	40	92.946	0.272
		1.2 Jy Sample			
10	0.864 ± 0.067	225	168	0.216	0.058
20	0.310 ± 0.039	96	120	94.926	0.031
30	0.156 ± 0.031	120	104	13.782	0.017
40	0.095 ± 0.025	150	88	0.004	0.019
60	0.057 ± 0.022	33	40	78.327	0.033
		PSC Samples			
10	0.889 ± 0.059	179	184	58.199	0.055
20	0.322 ± 0.035	124	136	75.696	0.023
30	0.152 ± 0.027	96	104	71.215	0.021
40	0.094 ± 0.023	123	88	0.817	0.014
60	0.048 ± 0.018	36	24	5.867	0.028
		PSC + FSS Samples			
10	0.881 ± 0.050	479	451	17.886	0.041
20	0.322 ± 0.030	469	403	1.281	0.023
30	0.154 ± 0.024	519	355	0.000	0.022
40	0.107 ± 0.024	517	307	0.000	0.012
60	0.055 ± 0.019	205	147	0.109	0.029

ume limiting, one grid did produce a variance as high as the E90 variance at $40h^{-1}$ Mpc. Notice that the scatter between grids is always comparable to our quoted error (i.e. roughly the maximum likelihood error from a single grid). The explanation for the high E90 variance at $40h^{-1}$ Mpc given by Efstathiou (1995) is that there was an upward statistical fluctuation in the number of QDOT galaxies in Hercules. We believe that this fluctuation had a bigger impact on the E90 analysis than on ours partially because we used multiple grids and partially because we removed the selection function bias.

The 1.2 Jy results, on the other hand, appear slightly larger than the results of Fisher *et al.*(1994). This may be due to differences in the masks.

In comparing estimates of clustering from different surveys we can assume that the ratio of variances is independent of scale and use a weighted average of the log of this ratio (with associated χ^2 and ν) to estimate $b_a/b_b = \sqrt{\sigma_{\rm a}^2/\sigma_{\rm b}^2}$. We find $b_{\rm QDOT}/b_{1.2\ {\rm Jy}} = 0.98 \pm 0.06$, $b_{\rm FSS}/b_{1.2\ {\rm Jy}} = 1.03 \pm 0.06$ and $b_{\rm FSS}/b_{\rm QDOT} = 1.06 \pm 0.07$. All have acceptable χ^2 values (indicating that the scale independence is justifiable) and on each scale the variances between surveys are consistent. All are consistent with $b_a/b_b = 1$ and in addition there is no significant disagreement between the variances measured by the different surveys on any scale. This can be seen in Figure 2. This in turn justifies our combining the samples. (In these comparisons we have assumed that the errors from each survey are independent. The many galaxies in common between QDOT and 1.2 Jy suggest that they are not in fact independent so we have overestimated the errors in $b_{\rm QDOT}/b_{1.2\ {\rm Jy}}$. However, the true errors would need to be much smaller for the the surveys to disagree significantly.)

The agreement between QDOT and 1.2 Jy is slightly at odds with the conclusions of Tadros & Efstathiou's (1995) power spectrum analysis of the two surveys. They find a discrepancy between the two surveys which disappears after the exclusion of the Hercules region. Their analysis uses a selection function derived from the 60μm luminosity function (Saunders *et al.*1990). It is possible that their analysis is more sensitive to the Hercules anomaly as a result of errors in this selection function. At the distance of Hercules, errors in the evolutionary term of the Saunders *et al.*(1990) luminosity function contribute a systematic 7.5 per cent uncertainty to their selection function. Our analysis is independent of the selection function. Differences between the mask used by Tadros & Efstathiou and the one we use could also have affected this comparison, by excluding significant features in one or other analysis.

A more detailed comparison of the 1.2 Jy survey and QDOT survey shows that they are consistent with a single underlying density field (Efstathiou 1995).

We can apply the same test to compare the variances of these surveys with the standard CDM variances quoted by E90. For none of the surveys does the weighted ratio of galaxy to CDM variances provide an acceptable fit at around 99 per cent significance. Using the full IRAS sample we find a weighted average $b_{\rm IRAS}/b_{\rm CDM} = 0.95 \pm 0.02$ (this average is dominated by the smallest scales). The fit is bad, $\chi^2 = 17.0, \nu = 4$, allowing us to reject the CDM model at the > 99 per cent level. This is clearly shown in Figure 2 where the slope of the variances with scale from the combined IRAS data is clearly at odds with the CDM slope.

2.4 Comparison With Model Power Spectra

Theoretical clustering predictions in the linear regime are frequently expressed in terms of the power spectrum $P(k)$ or in dimensionless form $\Delta^2 \propto k^3 P(k)$. The quantity Δ^2 is defined as the variance per $\ln k$ i.e. $\Delta^2 \equiv d\sigma^2/d\ln k$. For a power law spectrum ($\Delta^2 \propto k^{n+3}$) the fluctuations within Gaussian spheres (radius R_G) is given by

$$\sigma^2 = \Delta^2(k) \quad (9)$$

$$k = \left[\frac{1}{2}(\frac{n+1}{2})!\right]^{1/(n+3)} \frac{1}{R_G}. \quad (10)$$

Figure 2. Counts in cells variance as a function of scale: Top: 1.2 Jy Survey - solid line and stars; QDOT Survey - dashed line and circles; FSS-z - dot/dash line and crosses. Bottom: Standard Cold Dark Matter (E90) - sold line and stars; all IRAS surveys together - dashed line and circles.

For cubical cells ($V = l^3$) the same expression applies but with $R_G \rightarrow l/\sqrt{12}$ (Peacock 1991). The theoretical predictions relate to the real-space mass fluctuations whereas the σ^2 we have calculated is for galaxies in redshift-space. A common assumption is that the real-space galaxy and mass variances are linearly related by a bias parameter b (see e.g. equation 12, below) i.e. $\sigma_m^2 = \sigma_g^2/b^2$, while the redshift-space/real-space distortions on large scales can be corrected for using the relation

$$\sigma^2_{\rm real} = \sigma_z^2 \left[1 + \frac{2}{3}\left(\frac{\Omega^{0.6}}{b}\right) + \frac{1}{5}\left(\frac{\Omega^{0.6}}{b}\right)^2 \right] \qquad (11)$$

(Kaiser 1987).

We also make a functional correction to the model power spectrum to provide an approximation to the non-linear evolution of the power spectrum (Peacock & Dodds 1994). In addition we use the Peacock & Dodds (1994) correction for the redshift-space distortions which accounts for small scale 'finger of god' effects (for this we assumed a pairwise velocity dispersion of 450 kms^{-1} added in quadrature with the redshift measurement error of 190 kms^{-1}).

Figure 3 shows the predicted Fourier amplitudes from the FSS-z sample, QDOT, the 1.2 Jy sample and the PSC-FSS sample, calculated from equations 10 and 11 and using the results from Table 3. We also show the expected results from the APM power spectrum inversion of Baugh & Efstathiou (1994). We have assumed that the linear IRAS bias is $b_I = 0.7$ and the optical APM galaxies have a bias of $b_o = 0.9$, consistent with the results of Section 3, below.

These results are compared with the Mixed Dark Matter (MDM) model, which has previously been shown to be in good agreement with large scale clustering data (Taylor & Rowan-Robinson 1992, Schaefer & Shafi 1992). The model shown has $\Omega_{HDM} = 0.15$ and $h = 0.5$, taken from the results of van Dalen & Shaefer (1992), and is normalized to the COBE spectrum assuming $n = 1$, yielding an effective quadrupole of $19.9 \pm 1.6\mu$K derived by Gorski *et al.*(1994). We have also plotted the scale invariant $n = 1$ Harrison–Zeldovich spectrum.

Figure 3 again shows that there is now broad agreement between QDOT, 1.2 Jy and the PSC-FSS surveys. The MDM model is a good fit to the APM data, although it appears to have a slightly steeper slope than the IRAS data. This fit could not be improved by increasing the proportion of hot dark matter (HDM) because, with the same COBE normalization, we would then predict too much power on all these scales. Improvements could be made, either by adjusting the primordial spectral index, or by introducing a scale dependent bias. There are a number of reasons why the small discrepancies between the MDM model and the IRAS data do not justify such fine tuning. First, there are a number of debatable assumptions that have been made in order to predict the non-linear, redshift-space power spectrum from a linear theory, real-space power spectrum. Secondly, the assumption of Gaussian fluctuations in the data analysis causes us to underestimate our errors as described above. Thus we would conclude that our data are not incompatible with the MDM model.

3 COMPARISON WITH OPTICAL

An interesting question in the study of large scale structure is how the clustering properties of different galaxy populations are related. Since the various structure formation theories such as CDM predict the mass distribution, whereas redshift surveys probe only the galaxy distribution, we need to know how these are related. If different classes of galaxies do not trace the same structures then clearly at best only some of these classes can be faithfully tracing the mass. With an increased understanding of how different classes are related we can hope to gain some understanding of how the galaxies relate to the mass. This question is particularly pertinent to the interpretation of flux limited redshift surveys where the mix of populations changes with both the flux limit and the redshift. Any survey that contains two (or more) populations with different clustering properties is inevitably going to produce ambiguous results dependent on selection functions of the classes involved and the scales being considered.

A very simple possible relationship between galaxy populations is that they linearly trace some underlying density

Figure 3. Square root of the Power spectrum, $\Delta(k)$, for the FSS-z (stars), QDOT (circles). 1.2 Jy (triangles) PSC-FSS (squares) and APM (open circles). The data points have been offset along the k axis for clarity. The curved solid line is the Mixed Dark Matter model with 15 per cent hot dark matter and $h = 0.5$, normalized to COBE, and corrected for nonlinear effects. The broken line is the linear spectrum. The straight solid line is the extrapolated scale invariant Harrison-Zeldovich spectrum. The data has been corrected for linear redshift space distortion in the small angle regime, and a linear bias of $b_I = 0.7$ for the IRAS galaxies and $b_O = 0.9$ for the optical APM galaxies.

field subject to finite sample errors, i.e.

$$\frac{1}{b_a}\frac{\delta\rho_a}{\bar{\rho_a}}(\mathbf{r}) = \frac{1}{b_b}\frac{\delta\rho_b}{\bar{\rho_b}}(\mathbf{r}) = \frac{1}{b_c}\frac{\delta\rho_c}{\bar{\rho_c}}(\mathbf{r}), \text{etc.} \quad (12)$$

(If the galaxy distributions were identical then obviously $b_a \equiv b_b$ etc..) A more general relationship could be expressed as

$$\frac{\delta\rho_a}{\bar{\rho_a}}(\mathbf{r}) = f\left(\frac{\delta\rho_b}{\bar{\rho_b}}(\mathbf{r})\right) \quad (13)$$

in which case the linear-biasing model would be the first order approximation in the case of small $\frac{\delta\rho}{\bar{\rho}}$. Under the assumption of linear-biasing one can use the ratio of clustering amplitudes and similar statistics for different galaxy classes to estimate the relative bias parameters [e.g. $\sigma_a^2/\sigma_b^2 = (b_a/b_b)^2$].

Comparisons of optical and infrared galaxy clustering have been made, but give conflicting answers. Babul & Postman (1990) compare IRAS galaxies and CfA galaxies in the first CfA slice and conclude that they are consistent with same underlying galaxy distribution outside the core of the Coma cluster (i.e. $b_O/b_I = 1$). The ratio of variances between the QDOT and APM-Stromlo surveys, $\sigma_O^2/\sigma_I^2 = 1.0 \pm 0.35$ (Loveday *et al.*1992) implies $b_O/b_I = 1.0 \pm 0.18$ (95 per cent confidence), while power spectra analysis suggest $b_O/b_I = 1.3$ (Peacock & Dodds 1994). Dynamical estimates of $\beta \equiv \Omega^{0.6}/b$ from IRAS samples lie between $\beta_I = 0.6$ and $\beta_I = 1.3$ with excursions to $\beta_I = 0.25$; optical estimates lie between $\beta_O = 0.4$ and $\beta_O = 0.75$ with earlier estimates as low as $\beta_O = 0.1$ (Dekel 1994). The ratio $\beta_I/\beta_O = b_O/b_I$ but the wide range of estimates allows $0.8 < b_O/b_I < 3.3$. Ratios of cross- and auto-angular-correlations between the UGC ESO and IRAS suggest $b_O/b_I = 1.4 \pm 0.1, b_O/b_I = 1.0 \pm 0.3$ or $b_O/b_I = 2.0 \pm 0.6$ depending on which correlation functions are compared (Lahav, Nemiroff & Piran1990). On small scales the 2 Jy/CfA cross-correlation amplitudes suggested $b_O/b_I = 2$, while $b_O/b_I = 1$ was found when comparing the 2Jy survey with the Southern Sky Redshift Survey (Strauss *et al.*1992). Fisher *et al.*(1994) found $b_O/b_I = 1.38 \pm 0.12$ when comparing σ_8 from the 1.2 Jy survey with the optical $\xi(r)$ of Davis & Peebles (1983).

We can use our estimates of the variance in cells together with that from an optical survey to estimate b_O/b_I. Using our PSC + FSS-z sample with the APM-Stromlo variances in cubic cells gives $b_O/b_I = 1.20 \pm 0.05$ with $\chi^2 = 1.2, \nu = 4$. This is consistent with some of the lower determinations above but rules out $b_O/b_I = 1$.

There are two problems with these analyses. First they do not test the underlying hypothesis that the distributions are linearly biased with respect to each other. Secondly the IRAS and optical classes are not clearly defined galaxy classes. What constitutes an IRAS galaxy depends on both the flux limit used and the redshift at which you find it, and the same is true of optical galaxies. Most notably a given galaxy can be seen in both optical and IRAS surveys.

In this section we are going to explore the relationship between the clustering of IRAS and optical galaxies taken from our FSS-z surveys and the CfA samples. By design, the FSS-z surveys overlap with the first three strips of the CfA 2 survey. We are thus in a position to compare density fields directly point-by-point, rather than by comparing global clustering statistics. We will define IRAS and optical galaxies such that the classes are unique (no optical galaxy can also be an IRAS galaxy) and on the basis of a physical distinction that (to first order) is independent of redshift.

3.1 The CfA and FSS-z Samples

The optical parent catalogue is the only published strip in the second CfA survey (de Lapparent *et al.*1986); i.e. $26.5\,\mathrm{deg} < \delta < 32.5\,\mathrm{deg}, 8^{\mathrm{hr}} < \alpha < 16^{\mathrm{hr}}$. The IRAS parent catalogue comprises the FSS-z samples discussed above, including all galaxies down to 0.2 Jy.

Since our aim is to compare the structures traced by different galaxies within the same volumes we must first restrict the two parent surveys to have the same areal profile. This means excluding CfA galaxies which lie within our FSS-z mask and also any FSS-z galaxies outside the CfA boundaries. These cuts leave us with 976 FSS-z galaxies and 854 CfA galaxies.

Of course many galaxies that appear in the CfA catalogue will also be found in the FSS-z. We identify all such pairs using a $3'$ search radius. If more than one partner is found for a given source the match is made on the basis of brightness, nearness etc. (the details of the duplicate removals are relatively unimportant since most duplicates are neighbouring galaxies). One of these pairs was found to have a much larger redshift in one catalogue and, since the angular separation was also large, this match was rejected as a chance projection. This matching left us with three catalogues: 554 galaxies seen *only* in the CfA 2 survey; 300 galaxies seen in both surveys; 676 galaxies seen *only* in the FSS-z surveys. These three catalogues are statistically inde-

pendent, in the sense that no galaxy appears in more than one sample.

We now require a more physically meaningful classification of 'IRAS' and 'optical' galaxies. The mix of galaxy types in our three samples depends to a large extent on the survey selection functions, for example a nearby elliptical may be seen in both surveys but a similar galaxy would be unlikely to be detected in the FSS-z sample at a greater distance. To obviate this problem we have introduced a 60μm, B magnitude colour cut which neatly divides the common sample into two. The colour chosen is simply the ratio of the respective survey limits i.e.

$$\frac{S_{60}}{0.2} = 10^{0.4(15.5-m_B)}. \tag{14}$$

Naturally all objects seen only in the FSS-z survey will have a colour that is more infrared than this limit and vice versa. The only dependence on redshift that is now present in our classification enters through the difference between the slopes of the spectral energy distributions around the 60μm and B-bands. Applying reasonable K-corrections at $z = 0.3$ this flux criterion corresponds to a cut at $L_B > 2L_{60}$ and although this cut is essentially arbitrary, it provides a much more appealing definition of an IRAS galaxy or optical galaxy than its presence or absence in a flux limited catalogue.

After applying this cut we arrive at two samples:

866(735) IRAS galaxies,
664(639) optical galaxies,

where the numbers in parentheses indicate those sources that have redshifts.

We already know that elliptical galaxies do not trace the same density field as other galaxies (Dressler 1980) and we also know that ellipticals are under-represented in IRAS sample (de Jong *et al.*1984). So a priori we would expect some difference between the clustering of these two surveys simply from this morphological effect. This will be particularly important in this comparison since the CfA strip is strongly dominated by the Coma cluster. We therefore create a further sample in which we restrict the optical galaxies to exclude all elliptical galaxies. To identify the ellipticals we use the morphological classifications in the CfA catalogue and exclude all types earlier than Sa. This gives us an optical-spiral sample with 269(267) galaxies.

3.2 Qualitative comparison

The Figure 4 shows the cone diagrams for the three subsamples described in Section 3.1. In the optical sample the most striking structure is the Coma cluster and 'Great Wall'. In the IRAS sample the Coma cluster is considerably less pronounced, although the 'wall' itself appears equally prominent. The difference in appearance of the Coma cluster between the two samples is easily explained; the optical sample contains more ellipticals which are preferentially found in rich clusters. Clearly the IRAS sample probes much deeper than the optical sample although they have similar numbers of galaxies (this is because of the breadth of the IRAS luminosity function) i.e. the IRAS galaxies are sparser. There is some indication of a second 'wall' at around 15000km s^{-1} in the IRAS sample. Although this feature is poorly sampled in the optical at this depth, nevertheless with the IRAS galaxies to guide the eye one can pick it out. Beyond 10000 km s^{-1} between 12^h and 13^h there appear to be some voids of low signal-to-noise ratio in the optical data, but these are much less pronounced or non-existent in the IRAS data. In the optical-spiral sample we see that the Coma cluster is far less significant (as we would expect). More detailed observations are strongly limited by the sparsity of the galaxies.

Compressing the cone diagrams in the tangential dimension increases the signal-to-noise ratio at larger radii (Figure 5). Here we can more clearly see the second wall in the IRAS sample and guided by that we see a second peak in the optical data. Notice that the peak corresponding to the 'Great Wall' is a single broad peak in the optical but has two peaks in the IRAS data. This arise from the difference in selection functions.

The cone diagrams above are dominated by the selection functions of the various samples. Dividing the volume into cells within concentric shells we can estimate $\rho/\bar{\rho} = n_i/\sum n_i$ for each class within each cell. In Figures 6, 7 we have plotted the densities of each cell as seen in the optical sample against the densities as seen in the IRAS sample. Since there is no overlap between cells all the data points are independent. We have not plotted error bars which would have confused the plot. It should be noted that the under-densities will usually have fewer galaxies and therefore larger errors. The general trend in these plots seems to be a steeper slope than would be expected for identical clustering, or even a linear-bias model with $b_O/b_I = 1.3$. On larger scales this appears to be true both above and below the mean density indicating that, in the optical, not only are the clusters more dense but also the voids are less dense. On scales of $5h^{-1}$ Mpc the IRAS density appears to be higher than the optical density for densities larger than the mean density. This might be explained by fingers of god which would tend to smear out the optical clusters.

3.3 Contingency Table

We now turn to a quantitative comparison between the two samples. This method was first discussed by Oliver (1993). Recently a similar but statistically more rigorous method was brought to our attention (Efstathiou 1995).

3.3.1 Method

The most obvious scheme to test is that the IRAS and optical galaxies cluster in *exactly* the same way (i.e. $b_O/b_I = 1$). Our null hypothesis is thus that the over-density in any given cell is independen of galaxy class. We divide our survey volume into shells and cells as we did for the counts in cells analysis. Under our null hypothesis we are at liberty to combine the samples to give a single estimate of the 'galaxy' over-density in any cell. From this estimated over-density and the observed over-densities in each individual class we construct a statistic, X^2, (Kendall & Stuart 1979) which we compute across the whole shell;

$$X^2 = \sum_{ij} \frac{(n_{ij} - n_{i\star}n_{\star j}/n)^2}{n_{i\star}n_{\star j}/n}. \tag{15}$$

Figure 4. Cone Diagram of FSS-z/CfA2 Strip 1 intersection. Top – IRAS Galaxies. Middle – optical galaxies. Bottom – optical-spiral galaxies.

Here n ($= \sum_{ij} n_{ij}$) represents the total number of galaxies from both surveys in a given shell. The subscript i refers to the individual cells in the shell and j to the galaxy class. We have employed the notation $n_{i\star} = \sum_j n_{ij}$ to represent the marginal distributions. Here we have implicitly assumed that the observed galaxies give us an estimate of the underlying galaxy-density field, and that the measured differ-

Figure 5. $N(z)$ diagrams. The top diagram shows the $N(z) = \rho(z)dV$ for the IRAS sample while the middle diagram shows the same for the optical Sample, the bottom diagram is the ratio between the two (together with a power-law fit) this gives us $\bar{\rho_I}/\bar{\rho_O}$ as a function of z, independent of clustering (if there is no relative biasing)

Figure 6. $\rho_O/\bar{\rho_O}$ v $\rho_I/\bar{\rho_I}$ diagram of FSS-z/CfA2 Strip 1 intersection. Densities are calculated in nearly cubical cells of sizes 5 (top) and 10 h^{-1} Mpc (bottom). The straight line would indicate identical clustering, the curved line would be followed in a linear-biasing model with $b_O/b_I = 1.3$. All points are independent so the scatter is real, to avoid confusion we have not plotted error bars.

ence in densities between the two populations is governed by Poisson statistics, i.e. that the additional error terms due to clustering (and cross-correlations between cells) cancel out. In this case X^2 is asymptotically distributed as χ^2 and, when summed over all shells, has $M-N$ degrees of freedom where M is the total number of cells and N is the number of shells.

Figure 7. As for Figure 6 but for scales 20 (top) and 30 h^{-1}Mpc (bottom).

3.3.2 Selection Function

As with the counts-in-cells analysis this analysis is affected by the selection functions of the samples. If the relative density of the two samples $\bar{\rho_I}/\bar{\rho_O}$ changes significantly across a shell then this will introduce spurious discrepancies between the optical and IRAS clustering. As before, we could volume limit each sample within each shell. This discards more galaxies than necessary and for this analysis our statistics are sensitive to the mean density. To avoid any bias we require $\bar{\rho_I}/\bar{\rho_O}$ to be constant over each shell. We can estimate this quantity neatly, without calculating either se-

lection function independently, and (in the case of no relative bias) independently of clustering. It is simply the ratio of the two $\rho(z)$ distributions as shown in Figure 5. We have fitted the observed ratio with a power law giving us $\bar{\rho_I}/\bar{\rho_O}(z) \propto (1+z)^{27}$. In any given shell we then randomly throw away galaxies from the most dense sample to give us a constant $\bar{\rho_I}/\bar{\rho_O}$ over that shell. This is very efficient since the errors are dominated by the least dense sample and in any case the gradients across a shell are small. Our results were not significantly affected by this correction.

3.3.3 Cells with few galaxies

Technically we can calculate X^2 for all cells where there is at least one galaxy in each class but the X^2 statistic is only distributed as χ^2 in the limit of large numbers so it is unwise to take those results at face value. To avoid the problem of poorly sampled cells requires some care. If we simply exclude cells with fewer than $n_{\rm lim}$ galaxies in any class we would end up biasing our results. This is because we would be excluding cells with a higher over density in the class which has the lower mean density, and thus concluding that the other population had more under-dense regions. It is thus clear that any thresholding has to be imposed on $\delta\rho/\bar{\rho}$ rather than n. We thus impose the limit

$$\frac{n_{i\star}}{n} > \frac{n_{\rm lim}}{\min(n_{\star j})}, \qquad (16)$$

where we have replaced $\delta\rho/\bar{\rho}$ by the estimator $n_{i\star}/n$. Now our limit, $n_{\rm lim}$, determines the smallest number of galaxies of the most sparse class that we would expect in any cell. The actual $\delta\rho/\bar{\rho}$ limit varies from shell to shell, allowing us to extract the maximum information from the surveys. These sparse cells still contain useful information, especially about the voids. Fortunately our null hypothesis allows us to group cells together. We choose to group sparse cells with their neighbour but one, rather than excluding them totally. We present results for $n_{\rm lim} = 1, 2, 3, 4, 5$.

3.3.4 Results

The results of our contingency table analysis are presented in Table 4. The probability $P(X^2, \nu)$ is that of obtaining a value of X^2 higher than that observed assuming our null hypothesis and that X^2 is distributed as χ^2 with ν degrees of freedom. One can see from this Table that the hypothesis that the optical galaxies and the IRAS galaxies are identically tracing the same underlying field is ruled out on scales $5-20h^{-1}$Mpc with a high level of significance ($\gg 99\%$). On the $30h^{-1}$Mpc with $n_{\rm lim} = 5$ it is impossible to rule out the null hypothesis, although the high χ^2 at smaller $n_{\rm lim}$ may hint that our statistics are too poor for this to be informative.

As stated before, we expect some discrepancy because of the over-representation of elliptical galaxies in optical surveys. In Table 5 we present the results after having excluded the CfA ellipticals. Here the story is markedly different. We are unable to exclude our null hypothesis for scales $5, 10, 20h^{-1}$ Mpc. At $30h^{-1}$ Mpc we can formally rule out our null hypothesis at the 95 per cent level. With only two degrees of freedom this result should be treated with caution.

Scale $/h^{-1}$Mpc	X^2	ν	$P(X^2,\nu)$ /%	$n_{\rm lim}$
5	86.6	49	0.07470	1
5	70.6	31	0.00640	2
5	49.1	18	0.01036	3
5	25.7	10	0.41861	4
5	26.3	8	0.09185	5
10	86.4	47	0.04046	1
10	68.3	33	0.02920	2
10	57.4	27	0.05782	3
10	39.8	19	0.34293	4
10	44.1	15	0.01071	5
20	41.7	17	0.07288	1
20	38.4	11	0.00677	2
20	37.4	9	0.00226	3
20	30.7	7	0.00702	4
20	28.8	6	0.00662	5
30	12.8	7	7.60401	1
30	11.5	6	7.37997	2
30	12.4	6	5.32677	3
30	12.9	5	2.43094	4
30	5.7	4	22.12649	5

Table 4. Contingency table analysis results. Under the null hypothesis that the optically selected galaxies trace the same field as the IRAS galaxies $P(X,\nu)$ gives the probability of obtaining X^2 higher than the observed value, assuming that X^2 is distributed as χ^2 (the statistic X^2 is defined in equation 15). $n_{\rm lim}$ is the threshold used in merging cells with few galaxies (equation 16).

We thus conclude that the detectable differences in clustering between these two surveys are mainly due to the higher proportion of ellipticals in the optically selected samples. It is nevertheless surprising that significant differences persist to large scales where we might have expected the overabundance of ellipticals in rich clusters to be of less importance. This could be because of the Coma 'finger of god' which is quite extensive in redshift space. Alternatively it might suggest that the morphology-density relation extends to large scales.

3.4 Relative Bias Ratio

The contingency table analysis described in Section 3.3.1 tests only a very particular linear-biasing scenario (where $b_O = b_I$). A more general model allows for a relative bias between the different samples (equation 12). An extension of the above method allows us to test this more general model. To allow comparison with estimates of b_O/b_I from other methods (see e.g. Section 3), we will consider a model where the optical over-density is a constant multiple (b_O/b_I) of the IRAS over-density.

We thus construct a series of null hypotheses that the two galaxy distributions are linearly biased with a given ratio of bias parameters. Since we have no direct measures of the underlying mass distribution we can only investigate the *ratio* of b_O/b_I. For clarity we will discuss the biasing of the two populations relative to an underlying mass distribution

Scale $/h^{-1}$Mpc	X^2	ν	$P(X^2,\nu)$ /%	$n_{\rm lim}$
5	54.1	48	25.35328	1
5	37.3	26	7.08115	2
5	16.9	15	32.49382	3
5	10.3	8	24.47746	4
5	8.6	7	28.36795	5
10	58.1	37	1.48361	1
10	19.8	22	59.62626	2
10	25.7	18	10.63065	3
10	25.1	15	4.90583	4
10	12.4	10	25.70629	5
20	16.7	11	11.59919	1
20	15.1	8	5.67010	2
20	8.5	6	20.18399	3
20	7.1	5	21.62374	4
20	6.2	5	28.38374	5
30	15.9	6	1.41893	1
30	14.5	5	1.27080	2
30	7.7	2	2.07805	3
30	10.5	2	0.51919	4
30	7.8	2	2.02121	5

Table 5. Contingency table analysis results. As for Table 4 except that the CfA ellipticals were excluded prior to analysis.

on the understanding that our results are only sensitive to b_O/b_I. We could test any given ratio, perhaps arising from a physical biasing theory, or a ratio observed from global statistical measures such as the $b/\Omega^{0.6}$ results from velocity fields. Alternatively we could run through a series of possible b ratios and see which are the most acceptable.

To incorporate this biasing ratio we must modify our X^2 statistic slightly, breaking away from a simple contingency table analysis. For each cell $\bar{n}_{ij}$ is estimated as $V_i \sum_i n_{ij} / \sum_i V_i$ and $\Delta n_{ij} = n_{ij} - \bar{n}_{ij}$ (V_i is the unmasked volume of cell i), then

$$\langle \frac{1}{b_j} \frac{\Delta n_{ij}}{\bar{n}_{ij}} \rangle = \frac{\delta\rho_m}{\bar{\rho}_m}. \tag{17}$$

We can thus estimate the underlying mass fluctuations in a cell by

$$\Delta_i = \frac{\sum_j w_{ij} \Delta n_{ij}/b_j \bar{n}_{ij}}{\sum_j w_{ij}} \tag{18}$$

We choose to use the mean densities of the two species as weights ($w_{ij} = \bar{n}_{ij}$). This weighting scheme means our analysis will agree with the contingency table analysis at $b_O/b_I = 1$. Other schemes are possible but they rely on the observed values in each cell and are not as robust.

We are then in a position to construct a new X^2 statistic

$$X^2 = \frac{\sum_{ij} (\Delta n_{ij}/b_j \bar{n}_{ij} - \Delta_i)^2}{{\rm var}(\Delta n_{ij}/b_j \bar{n}_{ij})}. \tag{19}$$

The variance is determined from Poisson statistics, neglecting errors and covariance terms arising from $\bar{n}_{ij}$ (in agreement with our contingency table analysis if $b_O/b_I = 1$):

$${\rm var}(\frac{1}{b_j} \frac{\Delta n_{ij}}{\bar{n}_{ij}}) = \frac{\Delta_i + 1/b_j}{b_j \bar{n}_{ij}}. \tag{20}$$

In the previous analysis we merged cells with an estimated under-density low enough that, for the class of galaxies with the lowest mean density at that shell, we would expect fewer than $n_{\rm lim}$ galaxies in that cell. With our new approach a similar argument introduces the following threshold

$$\Delta_i > \max_j (\frac{1}{b_j} \frac{n_{\rm lim} - \bar{n}_{ij}}{\bar{n}_{ij}}) \tag{21}$$

The results presented here have taken $n_{\rm lim} = 5$. The Δ_i limit varies with b_O/b_I, as does Δ_i itself so the number of cells merged depends on the value of b_O/b_I being tested.

We calculate the statistic X^2 for a range of $0.5 < b_O/b_I < 3$ and, under the assumption that this statistic is distributed as χ^2 with $M - N$ degrees of freedom, we calculate the probability $P(X^2, \nu)$ as before.

The results are presented in Figure 8 which shows the probability of obtaining a higher value of X^2 than that observed as a function of the assumed biasing ratio b_O/b_I. The curves in Figure 8 are for the four scales 5, 10, 20 and $30h^{-1}$ Mpc. The curves are not smooth because our cell merging threshold depends on the assumed bias ratio and jumps occur when new cells become merged. On scales of 5 to $10h^{-1}$ Mpc *all* linear-biasing models relating optical and IRAS galaxies can be ruled out with around 99 per cent significance. At the $5h^{-1}$ Mpc scale this is perhaps unsurprising since we are in the non-linear regime ($\delta\rho/\bar{\rho} > 1$) so a naive justification for a simple linear-biasing breaks down. Also on these smaller scales we expect that the 'fingers of god' (more prominent for the ellipticals in clusters) will have a non-linear impact on our analysis over and above any discrepancies in the over-densities. However, on scales of $10h^{-1}$ Mpc we might have expected that a linear-biasing model would have been reasonable. On larger scales (20 and $30h^{-1}$ Mpc) we do find that there are linear-biasing models that we cannot reject. A bias ratio of $1.7 < b_O/b_I < 3.3$ cannot be rejected with more than 95 per cent significance for $20h^{-1}$ Mpc cells and likewise $1.1 < b_O/b_I < 2.0$ is acceptable at $30h^{-1}$ Mpc. It is interesting that we can reject all $b_O/b_I < 1.7$ with more than 95 per cent confidence since it is within this region that most estimates of b_O/b_I lie (Section 3). Taken at face value this would imply that optical and IRAS density fields are not linearly related even on scales of $20h^{-1}$ Mpc.

Since we were unable to reject the hypothesis that $b_O/b_I = 1$ after the exclusion of optical ellipticals, we expect a wider range of acceptable bias ratios when comparing optical-spirals with the IRAS sample. This is indeed the case and for brevity we do not show the $P(X^2, \nu)$ plots for these samples. Suffice to say we cannot rule out $0.8 < b_O/b_I < 3$ between 5 and $20h^{-1}$Mpc (all linear-biasing models could be ruled out with 95 per cent confidence at $30h^{-1}$ Mpc but as before the few degrees of freedom at this scale cause us to be sceptical of this results).

4 CONCLUSION

We have completed two new large, deep IRAS redshift surveys. The large scale clustering properties of these surveys

have been analysed and found to be consistent with previous IRAS redshift surveys, strengthening previous conclusions that the IRAS galaxy distribution is inconsistent with the standard CDM predictions.

We noted two particular shortcomings in the counts-in-cells analysis. Firstly, the variances determined using different grid patterns on the same data show a scatter comparable with the quoted errors. Secondly the method is not completely independent of the selection function and we demonstrate one way of overcoming this bias.

We are able to combine all the IRAS samples together to obtain a single estimate of the variance on large scales with errors that will not be matched until the completion of the full PSC-z survey (Saunders *et al.*1995a; Saunders *et al.*1995b). Converting these variances into the form of a dimensionless power-spectrum (correcting for redshift-space distortions), we compare them with a mixed dark matter (MDM) model. The slope of this model spectrum appears slightly steeper than that observed but the assumptions involved in transforming theory to data are sufficiently uncertain that we can not read too much into this.

A comparison of our variance estimates with those from the APM-Stromlo redshift survey suggests $b_O/b_I = 1.20 \pm 0.05$, assuming a linear-biasing model with ratio independent of scale. This is higher than that found by the APM-Stromlo team themselves (Loveday *et al.*1992) because we find smaller IRAS variances than E90.

Using our FSS-z sample and the first CfA strip we directly compare the distributions of optical and IRAS galaxies (using a physically meaningful definition of the two classes). This is done on a point-by-point basis so we are able to test the hypothesis that the two populations are related by a linear-bias ratio (b_O/b_I).

We are able to reject the hypothesis that $b_O/b_I = 1$ with a very high degree of significance on the scales 5, 10 and 20 h^{-1} Mpc. This hypothesis is, however, acceptable if we exclude ellipticals and S0 galaxies from the optical sample, suggesting that the discrepancies are due to the morphology density relation and the under-representation of ellipticals in IRAS samples. On scales of 30 h^{-1} Mpc our conclusions would be reversed but we suspect that our statistics are too poor at this scale for this to be very meaningful.

Allowing b_O/b_I to vary away from 1 we find that only on the largest scales are *any* optical/IRAS linear-biasing models acceptable, if elliptical galaxies are included in the optical samples. Even on scales of 20 h^{-1} Mpc, linear-biasing with $b_O/b_1 < 1.7$ is ruled out with more than 95 per cent confidence. It should of course be stressed that in this particular volume the optical galaxy distribution is dominated by the Coma cluster and so the distorting effect of the elliptical galaxies has to some extent been amplified.

This non-linear clustering relation between ellipticals and IRAS galaxies may present complications for the interpretation of any galaxy surveys that include both elliptical and spiral galaxies. As yet we have been unable to determine any differences in the clustering properties of IRAS galaxies and spiral galaxies and so surveys composed of either of these can be meaningfully compared.

Figure 8. $P(\chi^2, \nu)$ v b_O/b_I for IRAS and optical galaxies on various scales.

ACKNOWLEDGMENTS

SJO and ANT acknowledge PPARC support. WS was supported by a PPARC Advanced Fellowship. We thank John Huchra, Ray Wolstencroft, Quentin Parker & Roger Clowes and Marc Davis & Michael Strauss for providing redshifts in advance of publication. We acknowledge use of the ING telescopes and thank the staff for their invaluable assistance. Much use has been made of the STARLINK resources.

REFERENCES

Babul, A., Postman, M., 1990, ApJ 359, 280
Baugh, C.M., Efstathiou, G., 1994, MNRAS 267, 323
Davis, M., Peebles, P.J., 1983, ApJ 267, 465
Dekel, A., 1994, ARA&A 32, 371
de Lapparent, V., Geller, M.J., Huchra, J., 1986, ApJ302, L1
de Jong, T., Clegg, P.E., Soifer, B.T., Rowan-Robinson, M., Habbing, H.J., Houck, J.R., Aumann, H.H., Raimond, E., 1984, ApJ 278, L67
Dressler, A., 1980, ApJ 236, 351
Efstathiou, G. MNRAS(in press)
Efstathiou, G., Kaiser, N., Saunders, W., Lawrence, A., Rowan-Robinson, M., Ellis, R.S., Frenk, C.S., 1990, MNRAS247, 10p
Fisher, K.B., Strauss, M.A., Davis, M., Yahil, A. and Huchra, J.P., 1992, ApJ 389, 188
Fisher, K.B., Davis, M., Strauss, M.A., Yahil, A. and Huchra, J.P., 1993, ApJ 402, 42
Fisher, K.B., Davis, M., Strauss, M.A., Yahil, A. and Huchra, J.P., 1994, MNRAS 266, 50
Fisher, K.B., Huchra, J.P., Strauss, M.A., Davis, M., Yahil, A. and Schlegel, D. 1995, ApJS100, 69
Gorski, K.M., Hinshaw, G., Banday, A.J., Bennett, C.L., Wright, E.L., Kogut, A., Smoot, G.F., Lubin, P. 1994, ApJ430, L89
Kaiser, N., 1987, MNRAS 227, 1
Kaiser, N., Efstathiou, G., Ellis, R.S., Frenk, C.S., Lawrence, A., Rowan-Robinson, M. and Saunders, W., 1991, MNRAS 252, 1
Kendall, M.G. and Stuart, A. 1979, *The Advanced Theory of Statistics, Vol.2*, 4th ed. (Griffin)
Lahav, O., Nemiroff, R.J., Piran, T., 1990, ApJ 350, 11
Lawrence, A., Walker, D., Rowan-Robinson, M., Leech, K.J., Penston, M.V. 1986, MNRAS 219, 687
Loveday, J., Efstathiou, G., Peterson, B.A., Maddox, S.J., 1992, ApJ 400, L43
Moore, B., Frenk, C.S., Wienberg, D.H., Saunders, W., Lawrence, A., Rowan-Robinson, M., Kaiser, N., Efstathiou, G., and Ellis, R., 1992, MNRAS 256, 477
Moshir M., *et al.*, 1992, *Explanatory Supplement to the IRAS Faint Source Survey, Version 2.* JPLD-10015 8/92 (Pasadena: JPL)
Oliver, S. J., 1993, *Ph.D. Thesis.* University of London
Oliver, S., Broadhurst, T, Rowan-Robinson, M., Saunders, W., Lawrence, A., McMahon, R., Lonsdale, C., Hacking, P., Taylor, A., Conrow, T. 1995, in Maddox, S.J., Aragon-Salamanca, A. eds, Proceedings of the 35th Herstmonceux Conference, Wide-Field Spectroscopy and the Distant Universe, World Scientific, Singapore p. 264
Peacock, J.A., 1991, MNRAS 253, 1p
Peacock, J.A., Dodds, S.J. 1994, MNRAS 267, 1020
Rowan-Robinson, M., Broadhurst, T., Lawrence, A., McMahon, R.G., Lonsdale, C.J., Oliver, S.J., Taylor, A.N., Hacking, P.B., Conrow, T., Saunders, W., Ellis, R.S., Efstathiou, G.P., Condon, J.J. 1991, Nat 351, 719
Rowan-Robinson, M., Walker, D., Chester, T., Soifer, T., Fairclough, J. 1986, MNRAS 219, 273
Saunders, W., Sutherland,W.J., Maddox,S.J., Oliver,S.J., Keeble,O.J., McMahon,R.G., White,S.D.M., Frenk,C.S., Rowan-Robinson,M., Tadros,H., Efstathiou,G., Smoker,J.V. 1995a, in C.Baltowski and R.C.Kraan-Kortweg eds, 3rd DAEC conference, ASP 67
Saunders, W., Sutherland,W.J., Maddox,S.J., Oliver,S.J., Keeble,O.J., McMahon,R.G., White,S.D.M., Frenk,C.S., Rowan-Robinson,M., Tadros,H., Efstathiou,G. 1995b, in Maddox, S.J., Aragon-Salamanca, A. eds, Proceedings of the 35th Herstmonceux Conference, Wide-Field Spectroscopy and the Distant Universe, World Scientific, Singapore p. 88
Saunders, W., Rowan-Robinson, M., Lawrence, A., Efstathiou, G., Kaiser, N., Ellis, R.and Frenk, C.S., 1990, MNRAS 242, 318
Saunders, W., Frenk, C.S., Rowan-Robinson, M., Efstathiou, G., Lawrence, A., Kaiser, N., Ellis, R.S, Crawford, J., Xia, X.-Y. and Parry, I., 1991, Nat, 349, 32
Schaefer, R. K., Shafi, Q., 1992, Nat 359, 199
Strauss, M.A., Davis, M., Yahil, A., Huchra, J.P., 1992, ApJ 385, 421
Tadros, H., Efstathiou, G. 1995 MNRAS276 L45
Taylor, A.N., Rowan-Robinson, M., 1992, Nat 359, 396
van Dalen & Schaefer, 1992, ApJ 398, 33

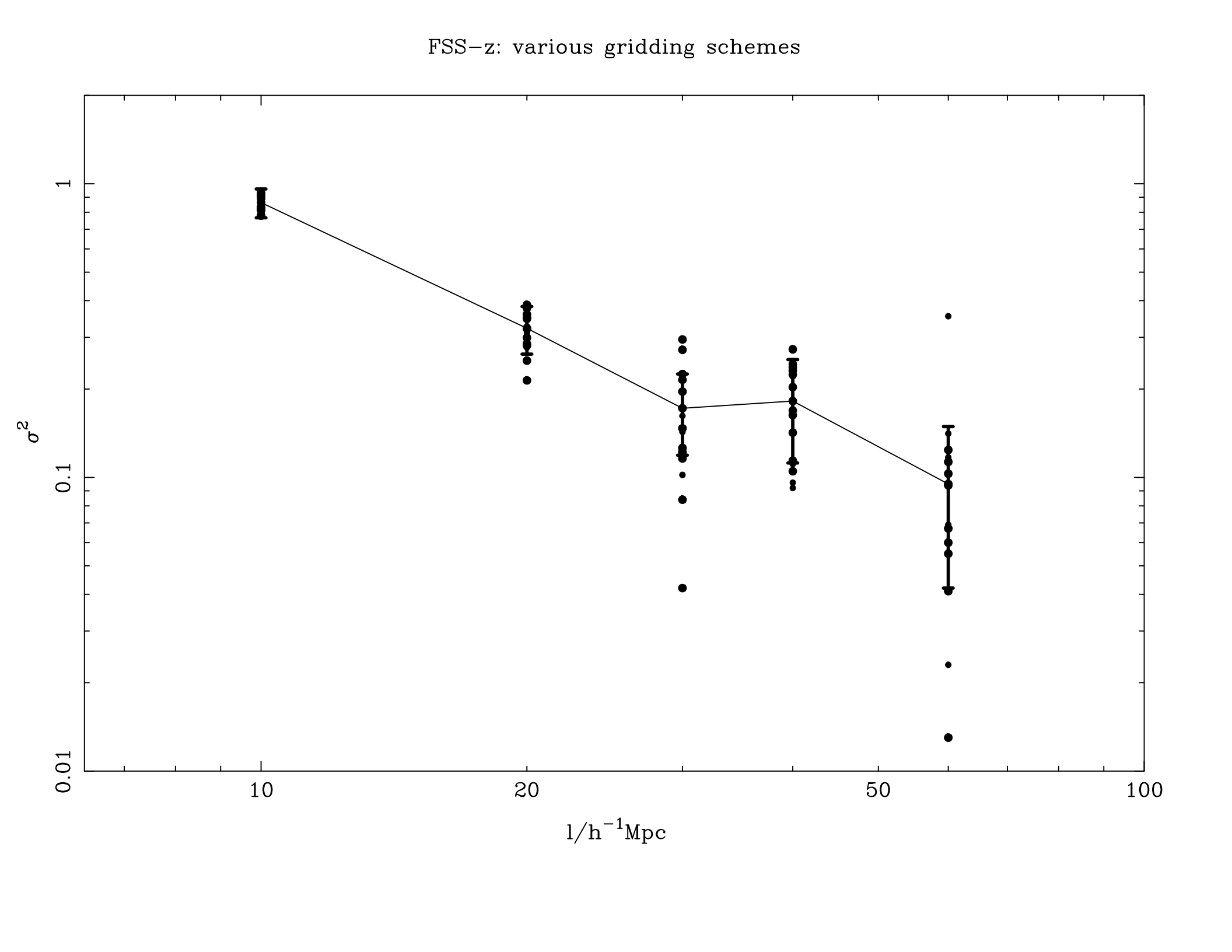
FSS−z: various gridding schemes
1
0.1
0.01
σ^2
10
20
50
100
l/h^{-1}Mpc

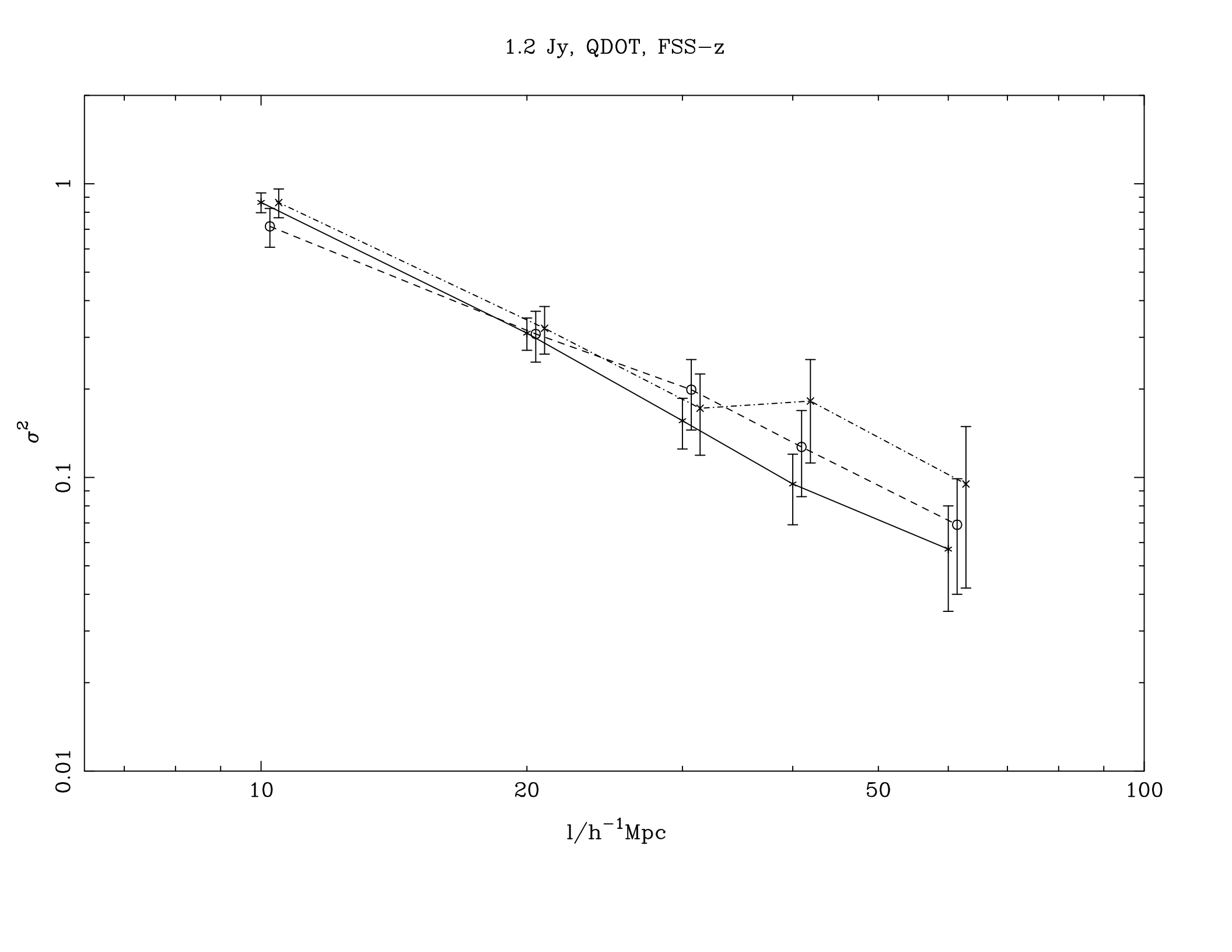
1.2 Jy, QDOT, FSS−z
1
0.1
0.01
σ^2
10
20
50
100
l/h^{-1}Mpc

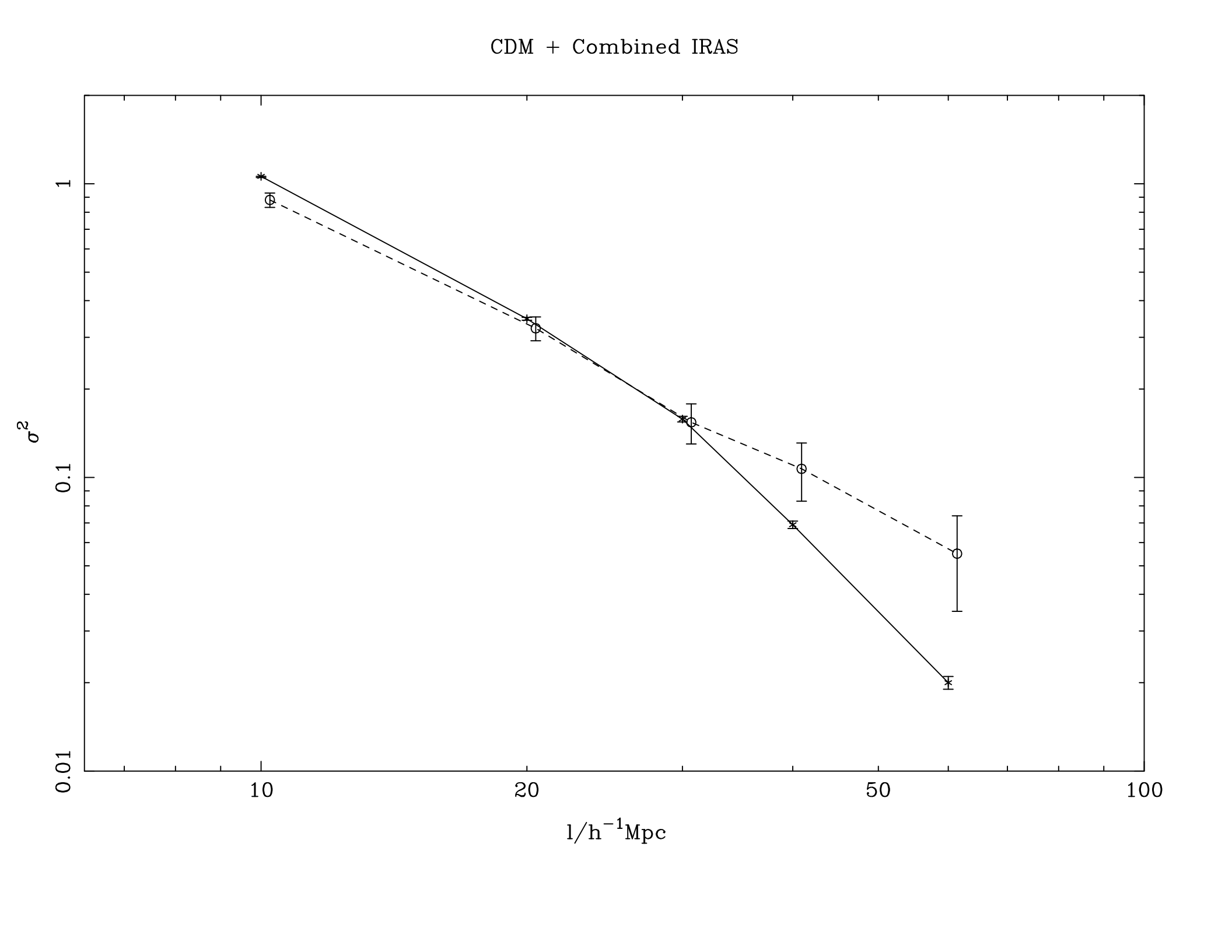
CDM + Combined IRAS
1
0.1
0.01
σ^2
10
20
50
100
l/h^{-1}Mpc

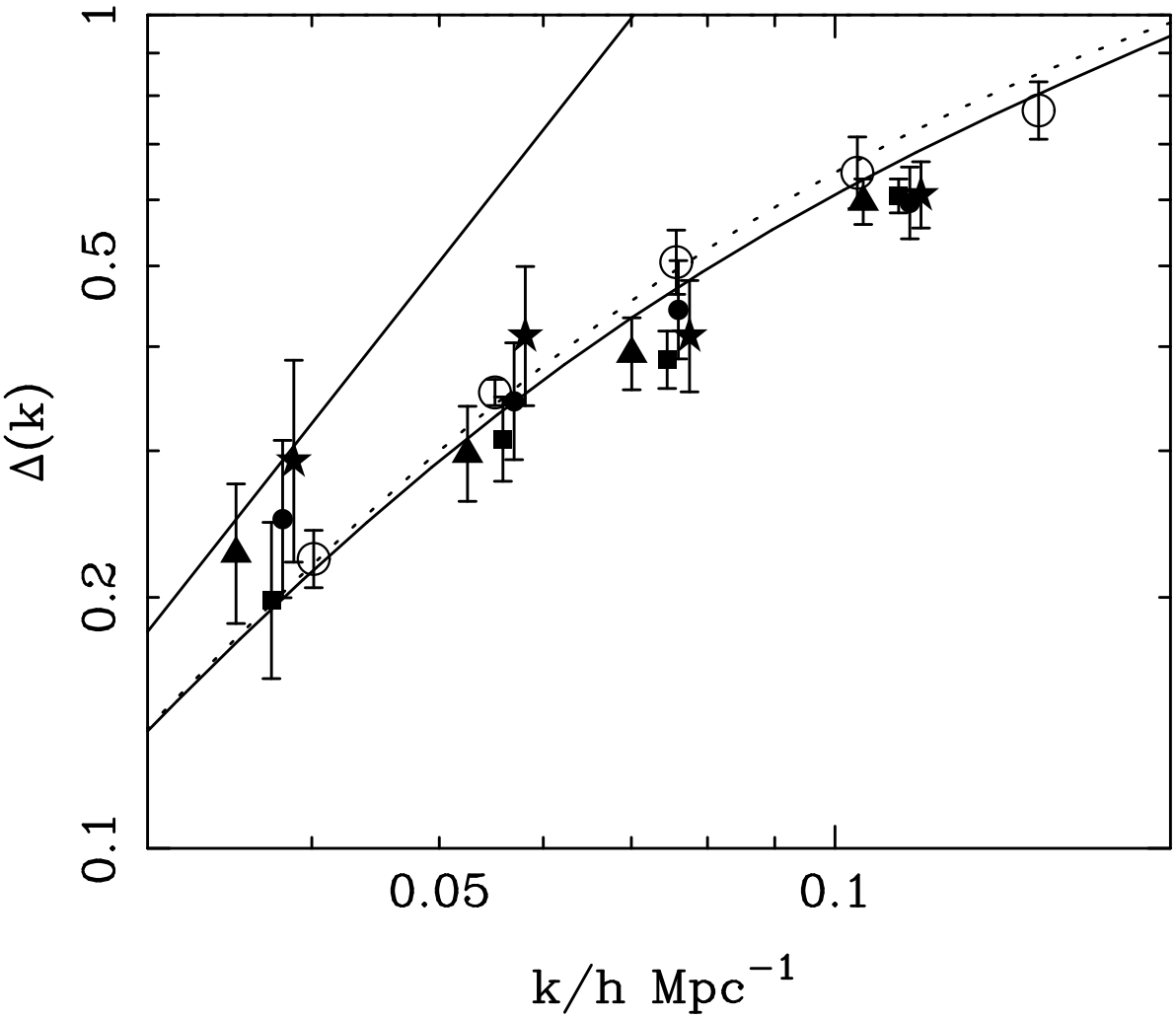
1
0.5
0.2
0.1
Δ(k)
0.05
0.1
k/h Mpc^{-1}

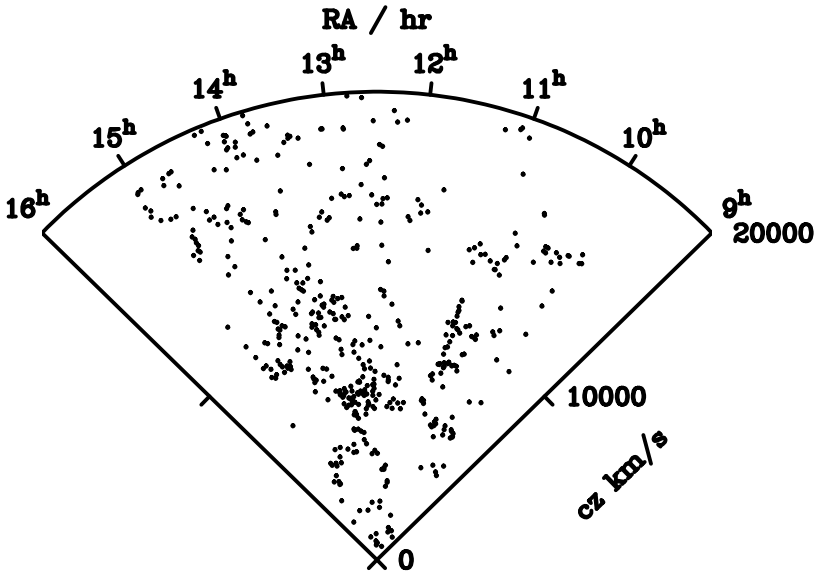

$26.5 < \delta < 32.5$

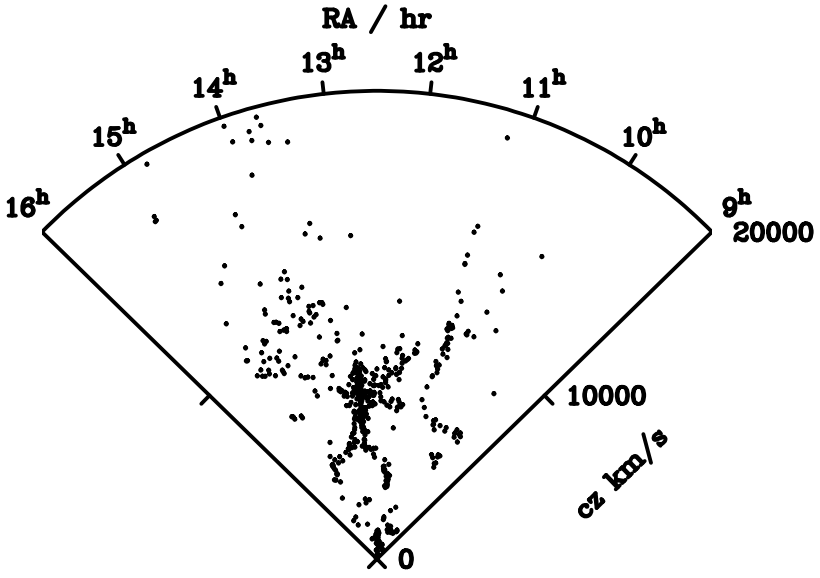

$26.5 < \delta < 32.5$

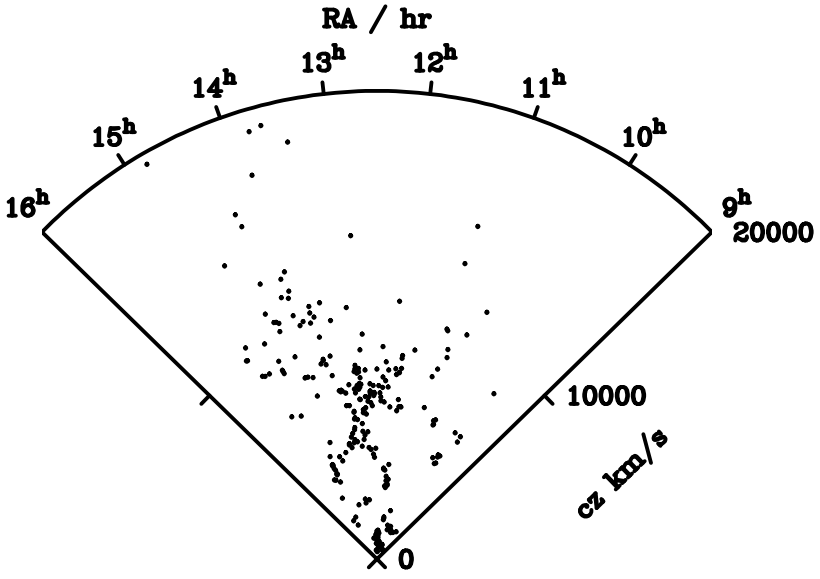

$26.5 < \delta < 32.5$

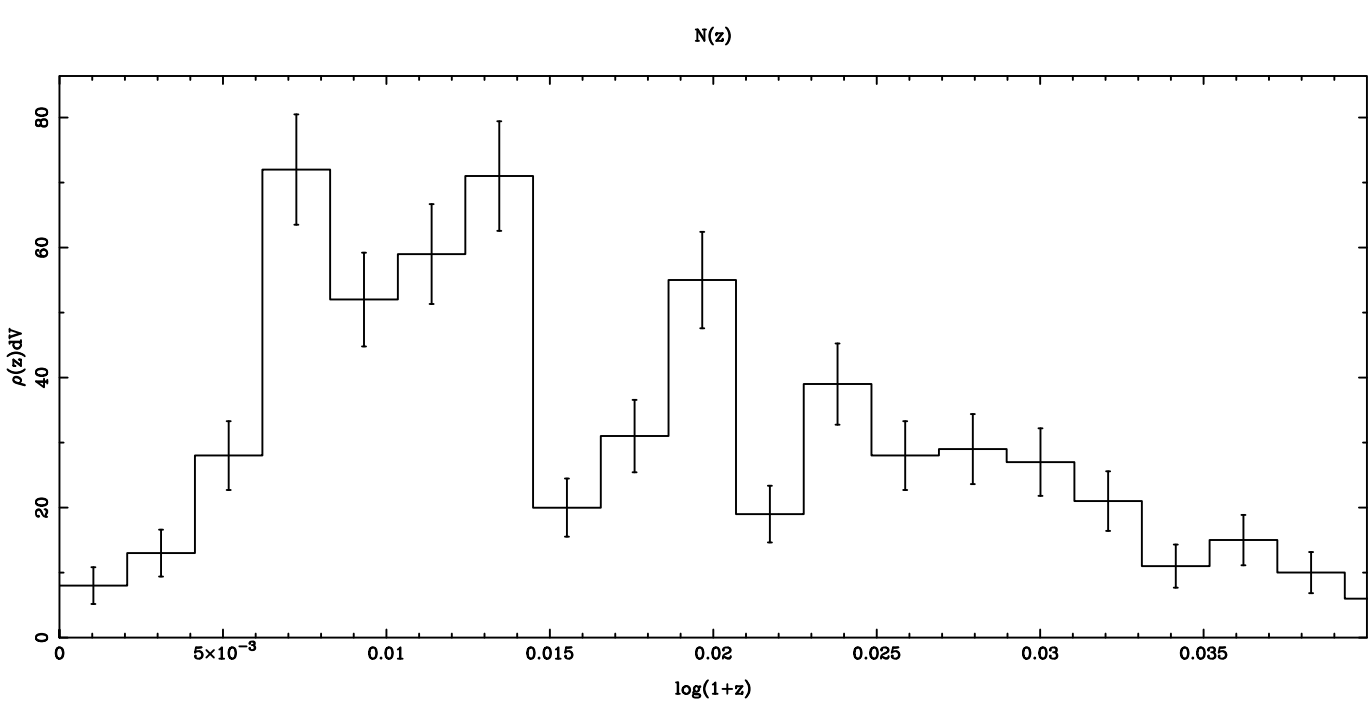
N(z)
ρ(z)dV
log(1+z)
0
20
40
60
80
0
5×10⁻³
0.01
0.015
0.02
0.025
0.03
0.035

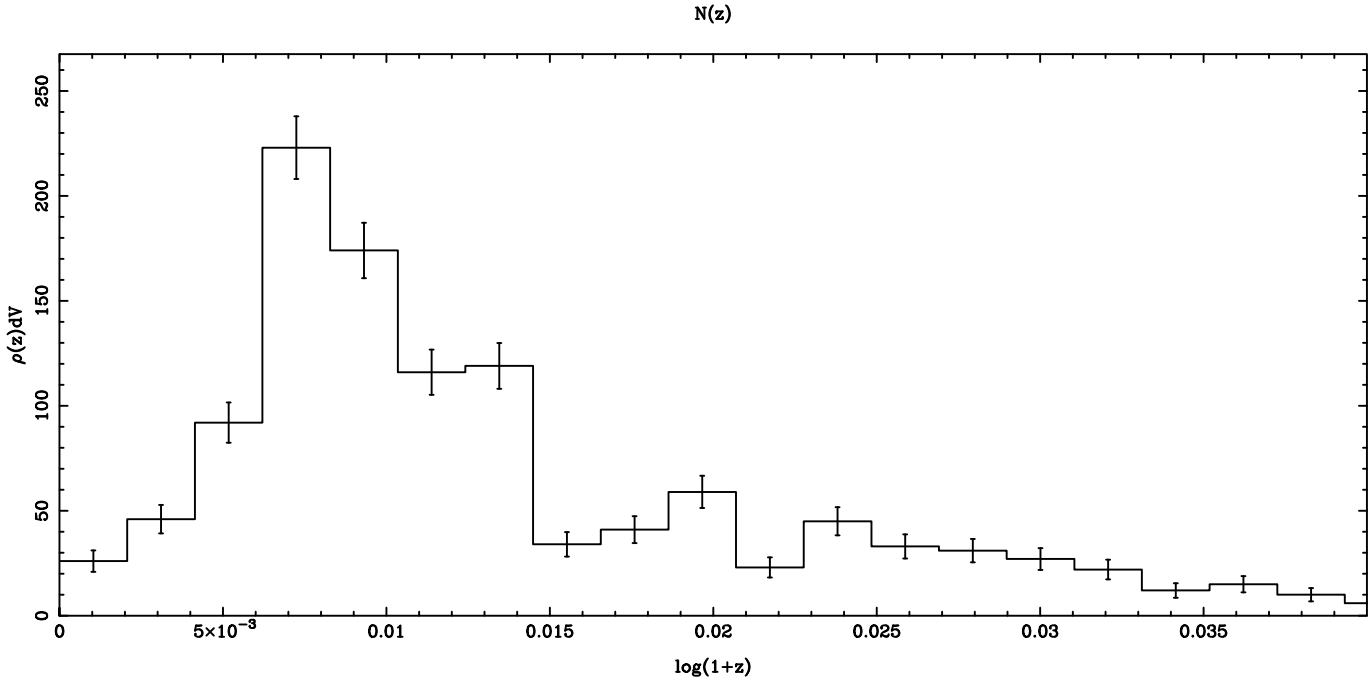
N(z)
ρ(z)dV
log(1+z)
0
50
100
150
200
250
0
5×10⁻³
0.01
0.015
0.02
0.025
0.03
0.035

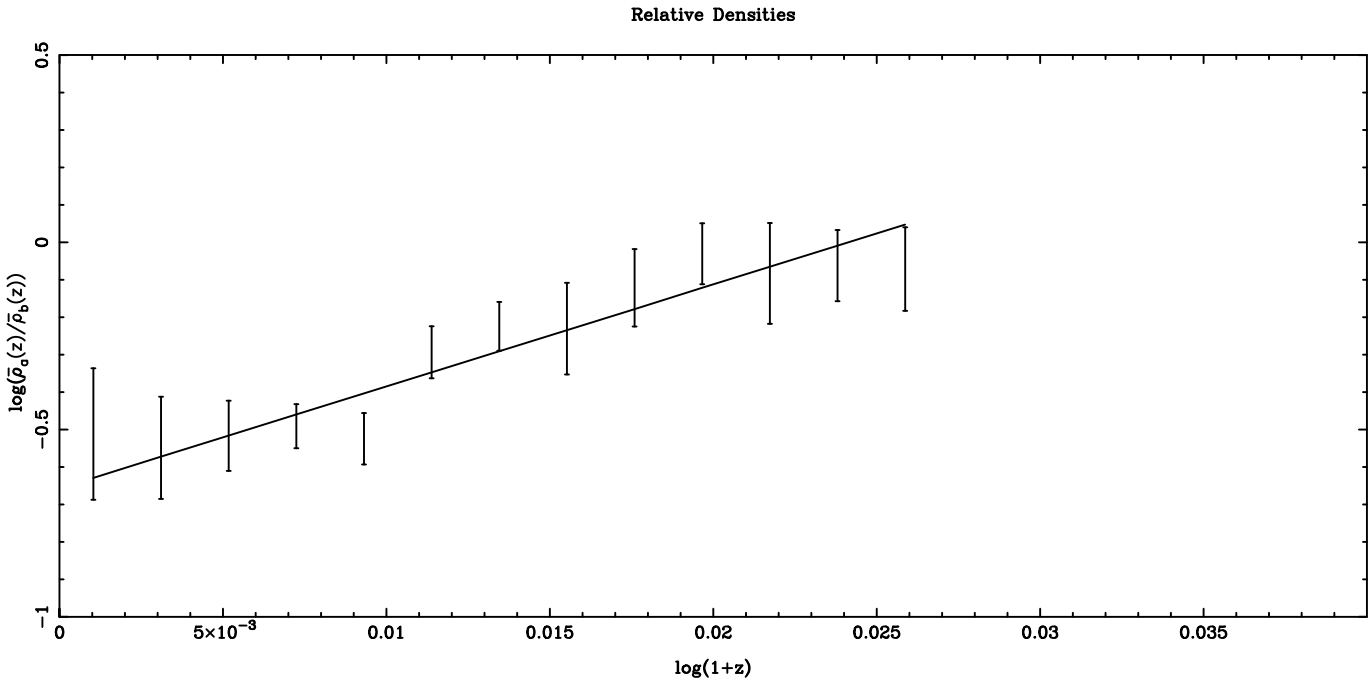
Relative Densities
log(ρ̄c(z)/ρ̄b(z))
log(1+z)
−1
−0.5
0
0.5
0
5×10⁻³
0.01
0.015
0.02
0.025
0.03
0.035

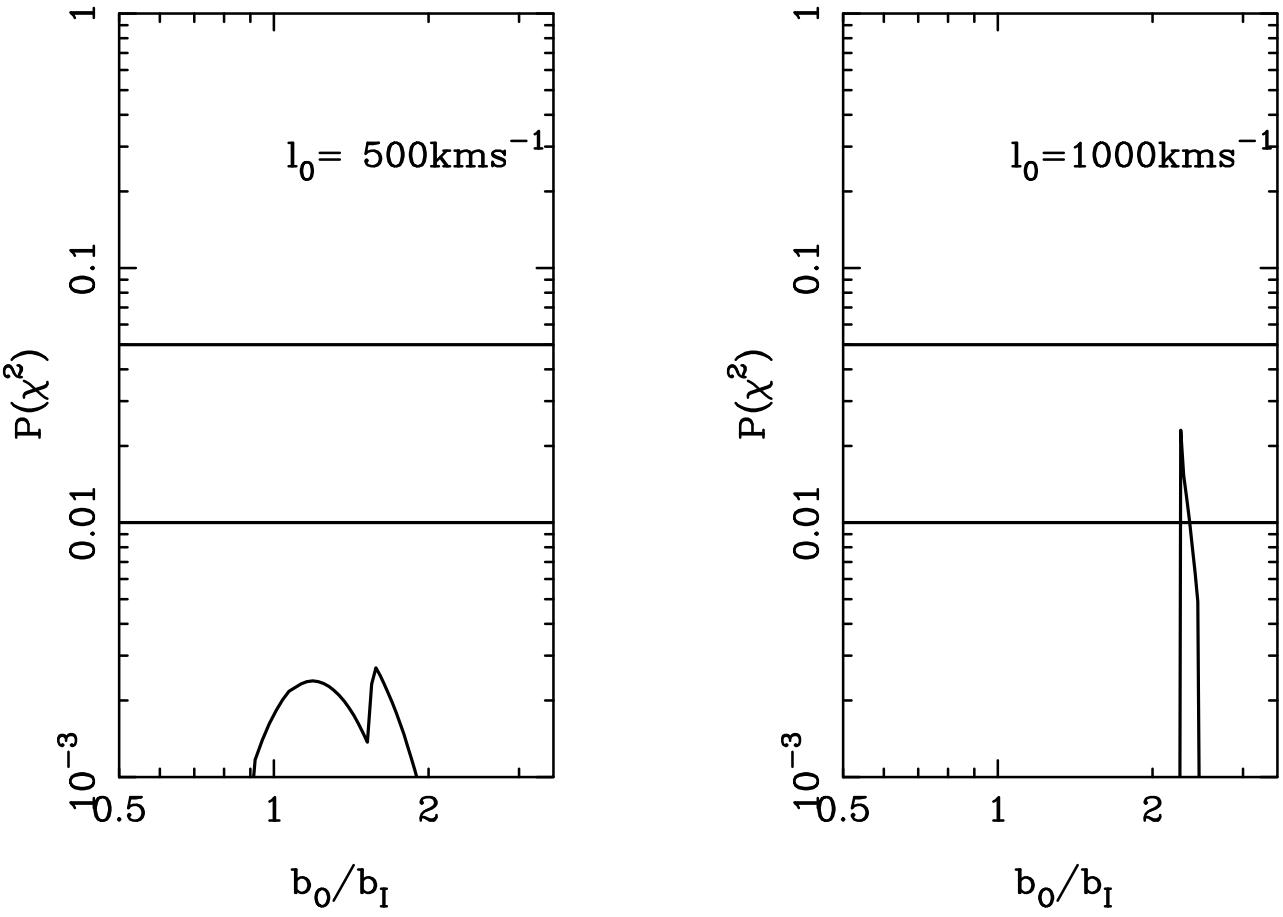
l_0= 500kms^{-1}
l_0=1000kms^{-1}
l_0=2000kms^{-1}
l_0=3000kms^{-1}
P(χ^2)
1
0.1
0.01
10^{-3}
0.5
1
2
b_0/b_I

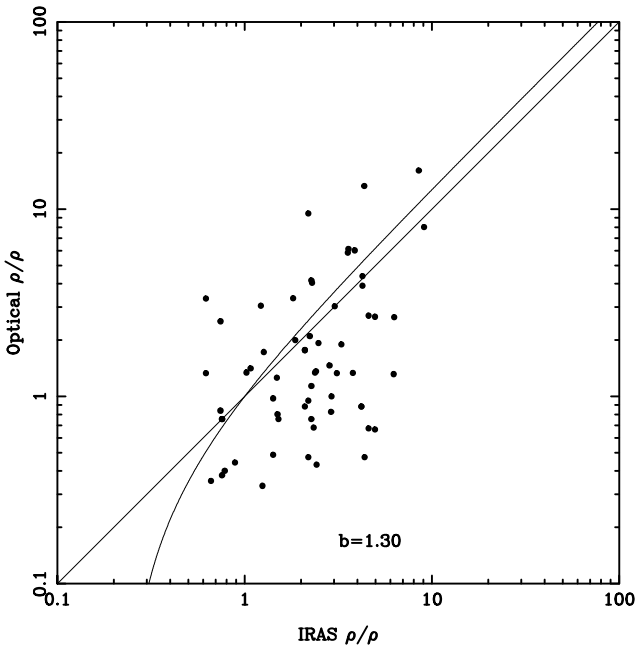
Optical ρ/ρ
IRAS ρ/ρ
b=1.30
0.1
1
10
100

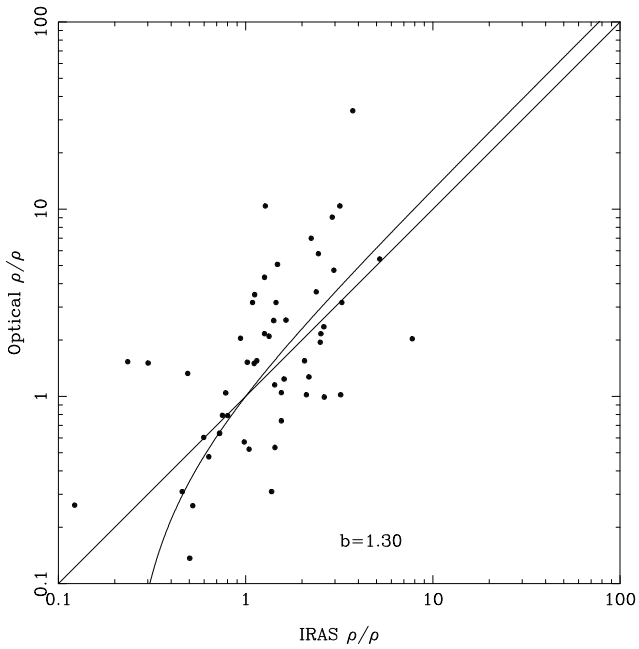
Optical ρ/ρ
IRAS ρ/ρ
b=1.30
0.1
1
10
100

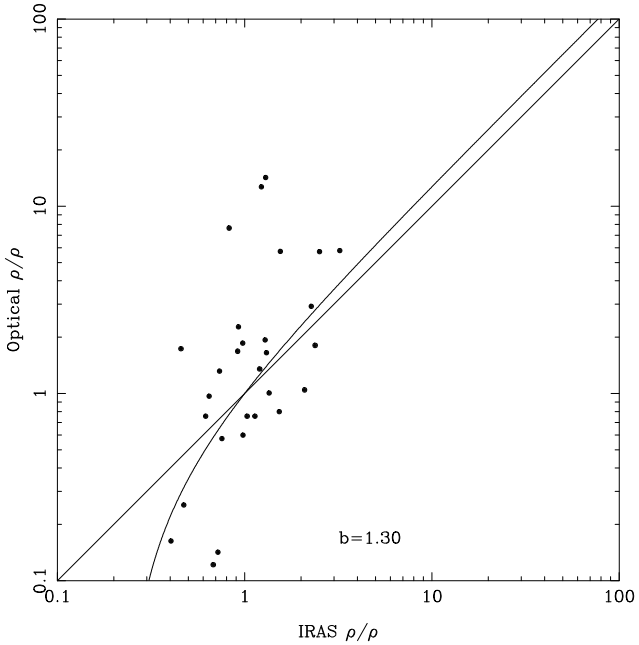
Optical ρ/ρ
IRAS ρ/ρ
b=1.30
0.1
1
10
100

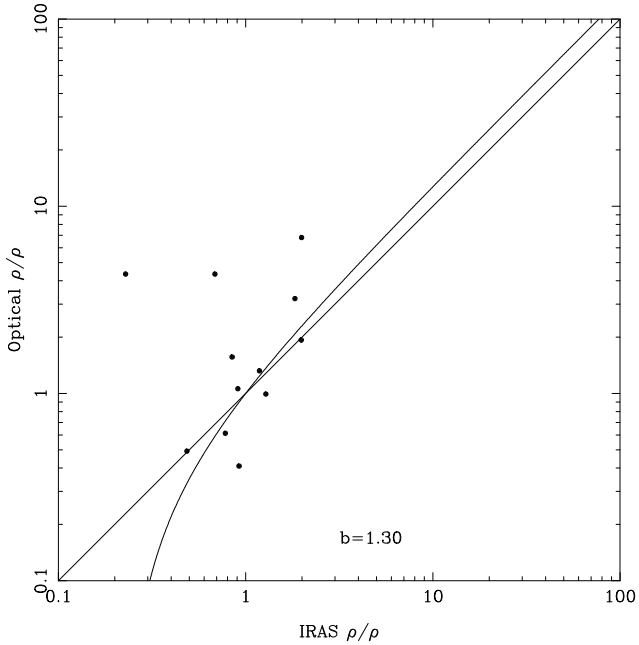
Optical ρ/ρ
IRAS ρ/ρ
b=1.30
0.1
1
10
100